Draft version November 23, 2017
Typeset using LaTeX **twocolumn** style in AASTeX61

THE INHOMOGENEOUS REIONIZATION TIMES OF PRESENT-DAY GALAXIES

Dominique Aubert,[1] Nicolas Deparis,[1] Pierre Ocvirk,[1] Paul R. Shapiro,[2] Ilian T. Iliev,[3] Gustavo Yepes,[4,5] Stefan Gottlöber,[6] Yehuda Hoffman,[7] and Romain Teyssier[8]

[1] *Observatoire Astronomique de Strasbourg,11 rue de l'Universite,67000, Strasbourg, France*
[2] *Department of Astronomy, University Texas, Austin, TX 78712-1083, USA*
[3] *Astronomy Center, Department of Physics & Astronomy, Pevensey II Building, University of Sussex, Falmer, Brighton BN1 9QH, United Kingdom*
[4] *Grupo de Astrofísica, Departamento de Fisica Teorica, Modulo C-8, Universidad Autónoma de Madrid, Cantoblanco E-280049, Spain*
[5] *Astro-UAM, UAM, Unidad Asociada CSIC*
[6] *Leibniz-Institute für Astrophysik Potsdam (AIP), An der Sternwarte 16, D-14482 Potsdam, Germany*
[7] *Racah Institute of Physics, Hebrew University, Jerusalem 91904, Israel*
[8] *Institute for Theoretical Physics, University of Zurich, Winterthurerstrasse 190, CH-8057 Zürich, Switzerland*

Submitted to ApJL

ABSTRACT

Todays galaxies experienced cosmic reionization at different times in different locations, since reionization was inhomogeneous. We show this by deriving the reionization (50% ionized) redshifts, z_R, of the intergalactic medium surrounding their progenitors, using fully-coupled radiation-hydrodynamics simulation of galaxy formation and reionization at $z > 6$, matched to N-body simulation to z = 0. Constrained initial conditions were chosen to form the well-known structures of the local universe, including the Local Group and Virgo, in a (91 Mpc)^3 volume large enough to model both global and local reionization. Reionization simulation CoDa I-AMR, by hybrid CPU-GPU code EMMA, used $(2048)^3$ particles and $(2048)^3$ initial cells, adaptively-refined, while N-body simulation CoDa I-DM2048, by Gadget2, used $(2048)^3$ particles, to find these reionization times for all galaxies at z = 0 with $M \geq 10^8 M_\odot$. Galaxies with $M(z=0) \gtrsim 10^{11} M_\odot$ reionized earlier than the universe as a whole, by up to ~ 500 Myrs, with significant scatter. For Milky-Way-like galaxies, z_R ranged from 8 to 15. Galaxies with $M(z=0) \lesssim 10^{11} M_\odot$ typically reionized as late or even later than global reionization at z=7.8, in neighborhoods where reionization was completed by external radiation. The duration of reionization was sometimes substantial, ranging as large as the range of reionization times. The Milky Way and M31 reionized earlier than global reionization, neither dominated by external radiation. Tracking their progenitors using either halos or particles yielded $z_R = 9.8$ (MW) and 11 (M31) or $z_R = 8.2$ (both), respectively.

Keywords: dark ages, reionization, first stars — galaxies: high-redshift — methods: numerical

Corresponding author: Dominique Aubert
dominique.aubert@astro.unistra.fr

1. INTRODUCTION

The emergent UV radiation field during the epoch of reionization (EOR) set the thermal and ionisation state of the intergalactic medium (IGM). It also suppressed baryonic infall and star formation in low-mass galaxies, through photoheating, especially for objects below $10^9 M_\odot$, limiting their contribution to reionization and causing reionization to self-regulate (e.g. Shapiro, Giroux, & Babul (1994), Iliev et al. (2007)). Accordingly, reconstructed star formation histories of the faintest dwarf galaxies indicate that reionization slowed their stellar population build-up (see e.g. Brown et al. (2014)). Recent large-volume, high-resolution, radiation-hydrodynamics (RHD) simulations of reionization also reproduce this suppression (Ocvirk et al. 2016).

Reionization was neither uniform nor instantaneous: large-scale structure created an inhomogeneous distribution of sources and absorbers. Different patches of the universe reionized at different times, over a wide range of redshifts.

This local reionization time left its imprint on galaxies at $z = 0$. The stellar populations of their satellites, for example, were dramatically affected by when reionization occurred and whether instantaneous or extended (see e.g. Koposov et al. (2009); Busha et al. (2010); Ocvirk & Aubert (2011); Iliev et al. (2011); Ocvirk et al. (2014); Gillet et al. (2015)). Reionization suppression is thought to reconcile the observed paucity of satellites in the Local Group (LG) with their over-prediction by N-body simulations of ΛCDM. In a global context, where the contribution of low-mass galaxies to reionization is still debated (see e.g. Bouwens et al. (2014); Finkelstein et al. (2015)), these effects must be understood in order to interpret observations of high-z galaxies.

We have modelled the inhomogeneous timing and duration of reionization as experienced by today's galaxies. The main challenge is to connect these objects to their progenitors during the EOR at $z > 6$, 13 billion years ago, by tracing their complicated mass-assembly histories to find the reionization histories of those progenitors. We combine for the first time a new, state-of-the-art, fully-coupled RHD simulation of galaxy formation and reionization at $z > 6$, with a dark-matter-only N-body simulation to $z = 0$, from the same initial conditions (ICs), to match galaxies at $z = 0$ with their reionization pasts self-consistently. Reionization simulation CoDa I-AMR ("Cosmic Dawn"), by hybrid CPU-GPU AMR code EMMA, used $(2048)^3$ particles and $(2048)^3$ initial cells, while N-body simulation CoDa I-DM2048, by Gadget2, used $(2048)^3$ particles, to find reionization times and durations for the galaxies in that volume at z = 0 with $M \geq 10^8 M_\odot$.

These ICs are a constrained realization of ΛCDM, constructed by the CLUEs ("Constrained Local UniversE Simulations") project from observations of galaxies in the local universe, to form familiar structures within it, including the LG with the Milky Way (MW) and M31 in a $(91\ \mathrm{Mpc})^3$ volume large enough to model both global and local reionization. These ICs enable us to model the reionization history of the LG in its authentic environment, to assess how representative it is, as the most accessible place to observe galaxies and their satellites today to deduce their histories.

The work presented here succeeds previous studies made by, e.g. Weinmann et al. (2007) or Dixon et al. (2017), who used radiative transfer to post-process pure N-body simulations. It also complements Alvarez et al. (2009) and Li et al. (2014), who focused on scales relevant to massive galaxies and clusters, using semi-numerical methodology. Thanks to the range of scales explored here (91 Mpc box-size sampled at kpc resolution), we are able to focus on smaller-mass objects between $10^8 M_\odot$ and $10^{13} M_\odot$. Our approach to matching present-day galaxies to their reionization past is similar to that in Ocvirk et al. (2014) on reionization of the LG. Here we model the EOR over the entire large-scale environment beyond the LG and compare the LG to the full population of galaxies. In addition, we simulate the EOR with fully-coupled RHD. The CoDa I-AMR simulation introduced here is a successor to simulation CoDa I of (Ocvirk et al. 2016). CoDa I-AMR has lower particle-mass resolution than CoDa I, but AMR makes its gravity length resolution comparable or better and compensates for the different initial grid-resolution of gas and radiation, while its star formation efficiency was re-calibrated to finish gobal reionization earlier, by $z = 6.1$.

We describe our simulations below and their analysis. We then present the reionization times and durations of our simulated population of galaxies, before discussing the LG.

2. METHODOLOGY

2.1. *Initial Conditions*

The CLUES constrained-realization ICs used here assume a WMAP 5 cosmology ($\Omega_m = 0.279, \Omega_v = 0.721, H_0 = 70$ km/s/Mpc, Hinshaw et al. (2009)) in a $(91\ \mathrm{Mpc})^3$comoving volume with 2048^3 particles and cells. These ICs are a coarsened version of those in the CODA I simulation (Ocvirk et al. 2016). Initial phases were chosen to reproduce the observed structures of the local universe at z=0, providing an MW - M31 pair with

the right mass range and separation in the proper large-scale environment (see Gottloeber et al. (2010), Iliev et al. (2011), Forero-Romero et al. (2011)).

2.2. *Reionization Simulation to $z = 6$*

EOR simulation CoDa I-AMR to $z = 6$, by hybrid CPU-GPU, AMR code EMMA (Aubert et al. 2015), solved fully-coupled equations of collisionless DM dynamics, hydrodynamics and radiative transfer, with standard sub-grid models for star formation and supernova feedback (Rasera & Teyssier (2006), Deparis et al. (2017)). The initial spatial grid of 2048^3 cells was refined whenever a cell contained more than 8 DM particles, until cell-widths reached 500 pc (proper), corresponding to three refinement levels by z=6, increasing total cell number by 2.1, to 18 billion. CoDa I-AMR was produced on Titan (ORNL) using 32768 CPU cores and 4096 GPUs dedicated to RHD solvers.

Star formation was triggered if gas overdensity in a cell exceeded 50, resulting in first star particles at $z \sim 19$; once triggered, star formation obeyed a Schmidt-Kenicutt Law with efficiency 1% (see Rasera & Teyssier (2006), Deparis et al. (2017)). Star-particles, of mass $7 \times 10^4 M_\odot$, released ionizing photons according to a Starburst 99 population model (Leitherer et al. 1999) with Top-Heavy IMF and 0.05 $Z_\odot$ metallicity; the corresponding emissivity was 1.5×10^{17} ionising photons/sec/stellar kg for 3×10^6 years, followed by exponential decline. A sugrid escape fraction 0.2 was applied to compute the photon number released inside the star-particle's cell. This ensured that global reionization finished at $z \sim 6$.

Radiative transfer was moment-based, with M1 closure and a reduced speed of light $c_{\rm sim} = 0.1$. Mechanical feedback from supernovae was included, with energy 9.8×10^{11} J/stellar kg injected into surrounding gas after 15×10^6 years: 1/3 via thermal energy, 2/3 via kinetic winds. At z=6, 120×10^6 star-particles were present.

Global reionization in CODA I-AMR finished by $z = 6.1$, with a reionization epoch consistent with CMB constraints (Planck Collaboration et al. 2015) but with a residual neutral fraction somewhat lower than expected from quasar data (Fan et al. (2006), see Fig. 1). The average star formation history was consistent with that inferred from observations of the UV luminosity function of high-z galaxies (Bouwens et al. 2014; Finkelstein et al. 2015).

2.3. *Dark-Matter-Only Simulation to $z = 0$*

The properties of z=0 halos were obtained from a dark-matter-only N-body simulation, CoDa I-DM2048, by Gadget2 (Springel 2005), from the same ICs as CoDa I-AMR, presented as simulation DM2048 in Ocvirk et al. (2016). Halos were identified using a FOF algorithm with linking length 0.2 and a minimum number of particles of 10, leading to $\sim$ 20 million halos identified at z=0. The smallest-mass FOF objects detected had $2.4 \times 10^7 M_\odot$. Merger trees were also generated to connect z=0 halos to their progenitors during the EoR (Riebe et al. 2013).

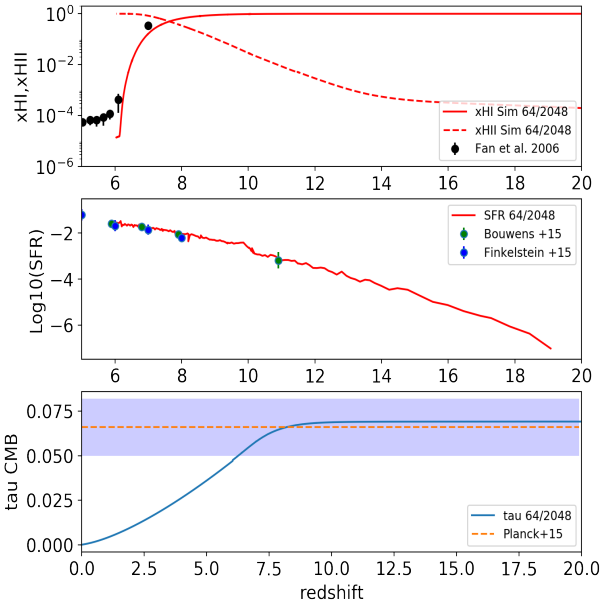

Figure 1. Globally-averaged results of CoDa I-AMR simulation vs. redshift: (top to bottom) volume-averaged ionized/neutral fraction, cosmic star formation rate ($M_\odot$/yr/Mpc^3), and CMB Thomson scattering optical depth.

2.4. *Reionization maps*

A 3-D map of reionization times (and redshifts) was created from the evolving, inhomogeneous, nonequilibrium ionization state of hydrogen in CoDa I-AMR. We define the reionization time as the instant when a cell first crossed the ionized-fraction threshold 0.5. The result is a 3-D field, $t_{\rm reion}(x, y, z)$, sampled using 2048^3 pixels corresponding to the base resolution of our simulation (see Fig. 2). There is a clear correlation between the CoDa I-DM2048 halo distribution at z=6 and the CODA I-AMR reionization map : halos are found at the centers of ionized patches and their spatial distribution matches the topology of $t_{\rm reion}(x, y, z)$.

This map was computed on-the-fly by EMMA with a time resolution driven by hydrodynamical processes. However, due to memory management issues, this pro-

cedure was stopped at $z = 8$, and, thereafter, reionization times were computed from stored snapshots of later time-slices. At its worst, time resolution was 1.4 Myrs at $z = 6$.

Cell-based reionization times do not distinguish cells inside galactic halos from intergalactic cells. It is the IGM, however, which undergoes reionization, while interstellar gas inside galaxies may remain neutral even after global reionization ends. It is, therefore, the reionization time of the IGM at the locations of the progenitor halos or particles we seek, specifically the times at which these locations first reached ionized fraction 0.5. Henceforth, this is what we shall mean when we assign a 'galaxy reionization time' $t_{\rm reion}$ to a $z = 0$ galaxy.

2.5. *Progenitor-based Reionization Times*

We start by assigning reionization times to $z = 0$ galaxies using those of their progenitor halos, using the merger-trees of the DM-only simulation to determine the positions, $\vec{x}_{\rm mm}$, at each $z > 6$, of their most-massive (mm) progenitors. Starting from $z = 20$, we find the earliest step in the merger tree when the most massive progenitor at that step belongs to an ionized cell. This step has redshift z_R, and the reionization time of a $z = 0$ halo is given by

$$t_{\rm prog} = t_{\rm reion}(\vec{x}_{\rm mmR}), \tag{1}$$

where $\vec{x}_{\rm mmR}$ is the center-of-mass position of the most massive progenitor of this halo at $z = z_R$.

A halo is assigned a reionization time only if it has a progenitor at $z > 6$; this is not the case if progenitor halos only emerged after $z = 6$ or were not detected by the FOF algorithm before this. However, this procedure guarantees that $t_{\rm prog}$ is set by material already in the structure by $z > 6$.

2.6. *Particle-based Reionization Times*

Our second approach is based upon the reionization times of all the DM particles that belong to a halo at $z = 0$. Once these particles are identified, their positions at $z > 6$ can be traced using simulation snaphots. Each particle is then assigned a reionization time defined as the earliest time $t(z_R)$ it was located inside an ionized cell in the reionization map. An average particle-based $\langle t_{\rm part}\rangle$ is then assigned to each halo:

$$\langle t_{\rm part}\rangle = \frac{\sum_{\vec{x}_{\rm p0}\in{\rm halo}}\ t_{\rm reion}(\vec{x}_{\rm pR})}{\sum_{\vec{x}_{\rm p0}\in{\rm halo}}\ 1}, \tag{2}$$

where $\vec{x}_{\rm p0}$ and $\vec{x}_{\rm pR}$ are particle positions at $z = 0$ and $z = z_R$, respectively.

This procedure is more difficult, as it requires cross-matching 8×10^9 DM particles with $\sim 20 \times 10^6$ $z = 0$ halos to identify the particles belonging to each halo. However, this technique has the advantage that it assigns reionization times to all $z = 0$ halos, even the smallest. Reionization times determined this way tend to be later than those by the other method since diffuse material, presumably reionized at later times and/or accreted after reionization, is included.

3. RESULTS

3.1. *Reionization Times*

Reionization times of z=0 halos are shown in Fig. 3. Galaxies with $M_{z=0} > 10^{11}h^{-1}M_\odot$ reionized up to 500 Myrs earlier than the full volume, depending on the method used. In this mass range, the more massive the galaxies, the earlier they reionized, as expected since their progenitors were located in denser environments where more intense sources formed. For lower masses, ($M_{z=0} < 10^{11}h^{-1}M_\odot$), reionization times were typically consistent with the global one. Their median time was slightly later than the global time : these objects were fainter or even star-less and were externally reionized. Since their immediate environment was denser than the average IGM, they ionized later than the IGM. Nevertheless, halo-to-halo scatter is significant ($\sim$ 250 Myrs $5\% - 95\%$ percentile).

Results for the two methods are consistent but different. The progenitor-based technique applies only to objects already formed at high z : it finds the reionization redshift of the oldest material of a z=0 halo, thus explaining why it consistently yields lower $t_{\rm reion}$. On the other hand, it requires that FOF objects pre-existed at $z > 6$, biasing the halo sample: $10^8h^{-1}M_\odot$ halos at z=0 must have had peculiar accretion rates to have progenitors at $z > 6$ and low mass at z=0. The dip in reionization times at the low-mass end confirms this, and our results indicate these objects are located in high-density regions, thus explaining their low $t_{\rm reion}$. It may also indicate these objects were more massive in the past and were stripped : these low-mass objects were assigned $t_{\rm reion}$ typical of more massive objects.

The particle-based method suffers less from this bias because all z=0 halos are included : the $t_{\rm reion}$ dip at the low-mass end disappears. It returns lower reionization redshifts for $M_{z=0} > 10^{11}M_\odot$, resulting from the fraction of material in halos at z=0 that was diffuse matter in the IGM and reionized at later times.

Li et al. (2014) found that $10^{12}h^{-1}M_\odot$ galaxies tend to reionize earlier than the IGM, by $\Delta z \sim 1 \pm 1$, while we find earlier reionization times for these objects, too, but by $\Delta z \sim 1.5 \pm 1.5$ (particle-based) or $\Delta z \sim 4.5 \pm 3$ (progenitor-based). The difference may be related to methodologies (excursion set formalism

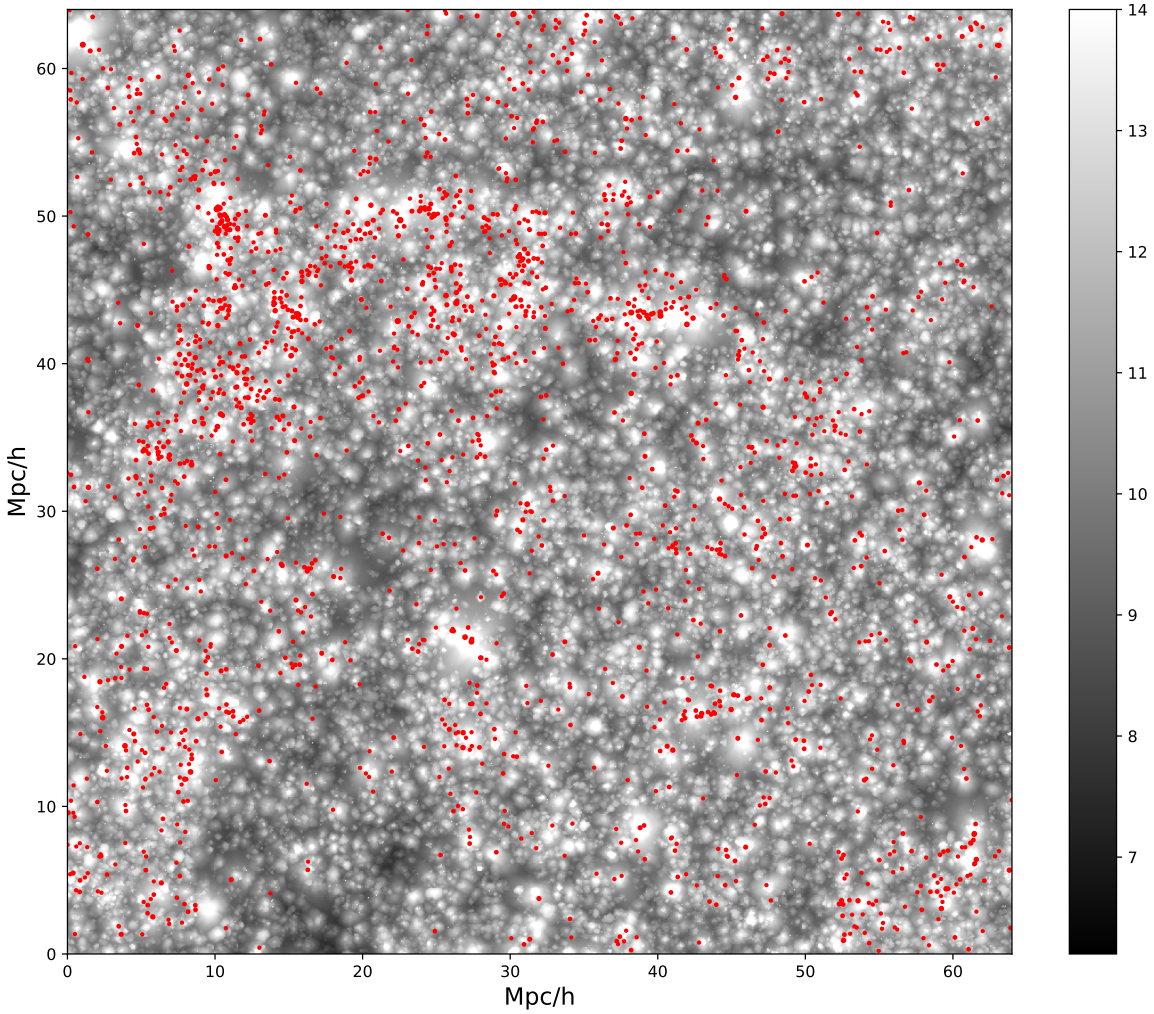

Figure 2. Projected distributions of the 2000 most massive halos in DM-only simulation CoDa I-DM2048 at z=6 (symbols) and the maximum values of the reionization redshift from CoDa I-AMR, along the projection axis.

against fully coupled RHD here) or earlier reionization histories driven by brighter sources (global 0.5 reionization redshifts $z_R \sim 11$ instead of 7.8 here) yielding smaller lags between galaxies and the IGM.

3.2. *Reionization Durations*

The spread Δt of reionization times $t_{\rm reion}$ of particles in a halo at $z = 0$ can be used to compute the duration of its reionization. The result is plotted versus halo mass in Fig. 3. $\Delta t_{2\sigma}$ is computed from the r.m.s. of particle reionization times within a halo, using $\Delta t_{2\sigma} = (\langle t_{\rm part}\rangle + \sigma) - (\langle t_{\rm part}\rangle - \sigma)$.

$\Delta t_{2\sigma}$ increases with halo mass, with typical values of $\sim$ 120 Myr for $M_{z=0} > 10^{11} h^{-1} M_\odot$. For $10^{12} h^{-1} M_\odot$, reionization durations as long as 180 Myr or as short as 60 Myr can be found. Ocvirk et al. (2014) made similar determinations for subhaloes of M31-MW analogs, and our results are consistent with their SPH model with similar emissivity for sources: our 120 Myr duration is typical of their reionization in isolated models, where inside-out reionization proceeds from inner regions of a galaxy to its outskirts. Our shortest durations, $\Delta t_{2\sigma} = 60$ Myr, are, on the other hand, typical of their externally-reionized scenario, where a nearby

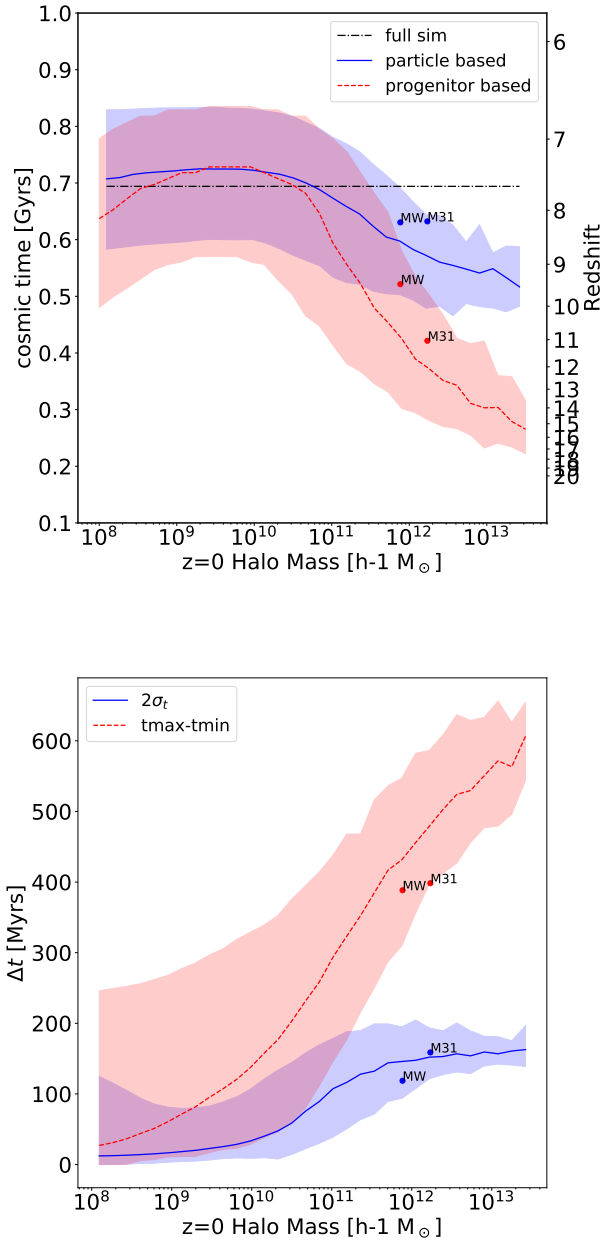

Figure 3. *Top*: Reionization times vs. present-day halo mass. Full volume reaches $x_{HI} = 0.5$ at $z \sim 7.8$ (dashed line). *Bottom*: Reionization durations Δt vs. present-day halo mass. In both panels, lines stand for the median value within each mass bin, and shaded areas span the $5\% - 95\%$ percentiles. Dots indicate the values for the simulated MW-M31 pair. See text regarding the different types of measurements.

bright source 'flashes' the object. The scatter here reflects diverse environmental properties.

For $M_{z=0} > 10^{11}h^{-1}M_{\odot}$, typical values of $\Delta t_{2\sigma}$ are comparable to the halo-to-halo scatter of $t_{\rm reion}$ and are likely to be lower bounds, since self-shielding may have been underestimated at our resolution limit. This is consistent with what Alvarez et al. (2009) and Li et al. (2014) found for more massive objects. Reionization was experienced at different times for different mass elements within any given present-day galaxy. This must be taken into account by any model of the impact of reionization on stellar populations.

At lower mass, $M_{z=0} < 10^{10}h^{-1}M_{\odot}$, objects have $\Delta t_{2\sigma} \sim 0$. This corresponds to extreme cases of fast external reionization or objects small enough to fit within a single cell of the reionization map (from AMR data smoothed to unrefined resolution $30h^{-1}$ comoving kpc, comparable to the virial radius of a $\sim 10^{9}h^{-1}M_{\odot}$ halo). Scatter increases toward the low-mass end, but these objects were sampled with a small number of cells or particles (40 particles for $10^{8}h^{-1}M_{\odot}$). Their environmental history is not as fully resolved, leading to greater errors estimating $\Delta t_{2\sigma}$.

$\Delta t_{2\sigma}$ estimates reionization durations from the spread of times for typical particles, but the full range of time differences within a halo can be even greater. The time difference $\Delta t_{\rm max-min}$ between the first and the last particle to reionize is also plotted in Fig. 3. The most massive halos can have $\Delta t_{\rm max-min} = 600$ Myr and thus contain material from locations that reionized at very different epochs.

Lower-mass haloes have smaller $\Delta t_{\rm max-min}$, with $\Delta t_{\rm max-min} \sim 400$ Myr for $10^{12}h^{-1}M_{\odot}$ but $\Delta t_{\rm max-min} < 100$ Myr for $M < 10^{10}h^{-1}M_{\odot}$. For the lowest-mass galaxies, significant outliers are present, with $\Delta t_{\rm max-min} \sim 200$ Myr when the median value is closer to 20 Myr.

3.3. *The Local Group*

Our CLUES ICs were constructed to form a LG, with two galaxies at $z = 0$ similar to the MW ($M_{z=0} = 7.7 \times 10^{11}h^{-1}M_{\odot}$) and M31 ($M_{z=0} = 1.7 \times 10^{12}h^{-1}M_{\odot}$) at their correct separation, surrounded by a realistic large-scale environment that matches observations of the local universe. Fig. 4 shows the positions of their progenitors at z=10.8 within the reionization map. The MW environment reionized in a compact fashion. The M31 reionization pattern, on the other hand, consists of several disconnected islands, reflecting the complex and extended distribution of progenitors at these times. Both objects reionized in isolation relative to each other: their patches are easily identified and disconnected. Ocvirk & Aubert (2011) and Gillet et al. (2015) predicted that this kind of reionization should lead to a more extended radial distribution of their satellites at z=0 compared to models without radiative transfer. The LG also reion-

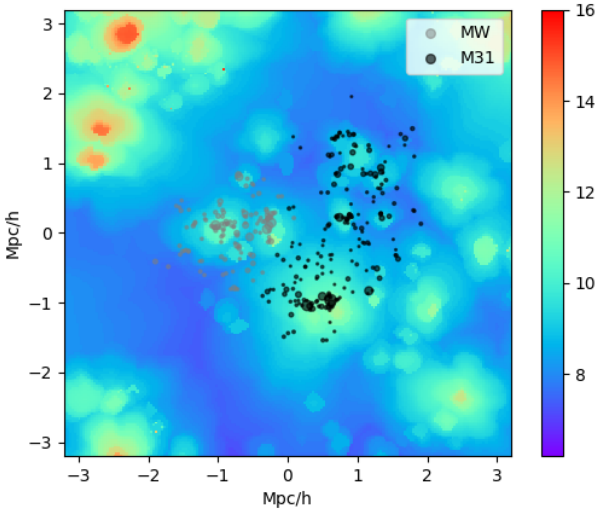

Figure 4. A slice thru the CoDa I-AMR reionization map around the LG (background field), with the location of CoDa I-DM2048 halo progenitors at z=10.8 for simulated M31 and MW (symbols). Symbol sizes are proportional to halo masses. Background colors indicate reionization redshift.

ized in isolation from the large-scale environment, as no ionization fronts appeared to sweep across them from outside.

In Fig. 3, their reionization times and durations are shown for each estimator. By the progenitor-based method, the M31 environment reionized earlier($z = 11$) than for MW ($z = 9.8$), consistent with the general trend whereby haloes more massive started reionization earlier. By the particle-based method, however, both objects reionized at the same time, at $z = 8.2$. Since these two objects are spatially close, it is not surprising that their Lagrangian environments reionized simultaneously. For both estimators, these two galaxies are typical for their masses, albeit on the 'late reionization' side of the distribution.

Regarding durations, $\Delta t_{2\sigma}$ are typical of the global distribution, between 100 and 150 Myr. $\Delta t_{max-min} \sim$ 400 Myr are similar for the two objects, indicating their environments share similar extreme values for reionization times, presumably because of their proximity.

These particle-based durations and times are consistent with the partially-suppressed model of Dixon et al. (2017), where low-mass galaxies $M < 10^9 h^{-1} M_\odot$ made a modest but non-negligible contribution to reionization : it suggests a similar quantitative role for such objects in CODA I-AMR.

4. SUMMARY

By combining a new, fully-coupled RHD simulation of reionization at $z > 6$ with an N-body simulation to $z = 0$ from the same ICs, we demonstrate that the redshifts at which present-day galaxies experienced reionization were correlated with their mass, by tracing their building-blocks back to the EOR. For $M_{z=0}$ between 10^8 and $10^{13} M_\odot$, galaxies more massive than the MW were typically reionized earlier than the global mean, with a spread in reionization times for the building-blocks of a galaxy as large as galaxy-to-galaxy variations. This inhomogeneous timing of reionization amongst and within galaxies should be taken into account when modelling and interpreting stellar populations. With CLUEs ICs, we modelled both global and LG reionization finding MW and M31 reionized earlier than the global mean, and mostly without influence from outside the LG or each other.

These results should be developed further in the future, as additional physical processes are included (e.g. possible AGN and X-ray binary sources, He and H_2 chemistry, metallicity evolution), limitations of numerical mass resolution and box size are overcome, and CLUEs ICs are improved by increased knowledge of the observed local universe.

DA, ND and PO acknowledge support from the French ANR funded project ORAGE (ANR-14-CE33-0016). PRS acknowledges the grant support of U.S. NSF AST-1009799, NASA NNX11AE09G, and DOE INCITE 2016 Award AST031 on the Titan supercomputer at Oak Ridge National Laboratory. ITI is supported by the UK Science and Technology Facilities Council [grant numbers ST/F002858/1 and ST/I000976/1] and The Southeast Physics Network (SEPNet).The CoDA I-DM2048 simulation was performed at LRZ Munich. GY would like to thank MINECO/FEDER (Spain) for financial support under research grant AYA2015-63810-P.

REFERENCES

Alvarez, M. A., Busha, M., Abel, T., & Wechsler, R. H. 2009, ApJL, 703, L167

Aubert, D., Deparis, N., & Ocvirk, P. 2015, MNRAS, 454, 1012

Bouwens, R. J., Bradley, L., Zitrin, A., et al. 2014, ApJ, 795, 126

Brown, T. M., Tumlinson, J., Geha, M., et al. 2014, ApJ, 796, 91

Busha, M. T., Alvarez, M. A., Wechsler, R. H., Abel, T., & Strigari, L. E. 2010, ApJ, 710, 408

Carlesi, E., Hoffman, Y., Sorce, J.,& Gottlber, S., 2017, MNRAS, 465, 4886

Chardin, J., Haehnelt, M. G., Aubert, D., & Puchwein, E. 2015, MNRAS, 453, 2943

D'Aloisio, A., McQuinn, M., Trac, H. 2015,ApJL, 813, L38

Davies, F. B. and Furlanetto, S. R.,MNRAS, 460, 1328

Deparis, N., Aubert, D., Ocvirk, P., & Gillet, N. 2017, submitted,

Dixon, K.,Iliev, I.,Gottlöber, S. Yepes, G. ,et al. 2017,arXiv:1703.06140

Fan, X., Carilli, C. L., & Keating, B. 2006, ARA&A, 44, 415.

Forero-Romero, J. E., Hoffman, Y., Yepes, G., et al. 2011, MNRAS, 417, 1434

Finkelstein, S. L., Ryan, Jr., R. E., Papovich, C., et al. 2015, ApJ, 810, 71

Gillet, N., Ocvirk, P., Aubert, D., et al. 2015, ApJ, 800, 34

Gottloeber, S., Hoffman, Y., & Yepes, G. 2010, ArXiv e-prints, arXiv:1005.2687

Hinshaw, G., Weiland, J. L., Hill, R. S., et al. 2009, ApJS, 180,225

Iliev, I. T., Mellema, G., Pen, U.-L., et al. 2006, MNRAS, 369, 1625

Iliev, I. T., Mellema, G., Shapiro, P. R., & Pen, U.-L. 2007, MNRAS, 376, 534

Iliev, I. T., Moore, B., Gottlöber, S., et al. 2011, MNRAS, 413, 2093

Koposov, S. E., Yoo, J., Rix, H.-W., et al. 2009, ApJ, 696, 2179

Leitherer, C., Schaerer, D., Goldader, J. D., et al. 1999, ApJS, 123, 3.

Li, T. Y., Alvarez, M. A., Wechsler, R. H., & Abel, T. 2014, ApJ, 785, 134

Ocvirk, P., & Aubert, D. 2011, MNRAS, 417, L93

Ocvirk, P., Gillet, N., Aubert, D., et al. 2014, ApJ, 794, 20

Ocvirk, P., Gillet, N., Shapiro, P. R., et al. 2016, MNRAS, 463, 1462

Planck Collaboration, Ade, P. A. R., Aghanim, N., et al. 2015, ArXiv e-prints, 1502, arXiv:1502.01589.

Rasera, Y., & Teyssier, R., 2006, A&A, 445,1

Riebe, K., Partl, A., Enke, H., et al. 2013, Astronomische Nachrichten, 334, 691

Shapiro, P. R., Giroux, M. L., & Babul, A. 1994, ApJ, 427, 25

Springel, V. 2005, MNRAS, 364, 1105

Weinmann, S., Maccio, A., Iliev, I., et al. 2007, MNRAS, 381,367

Wise, J. H., & Cen, R. 2009, ApJ, 693, 984